RSC Advances

PAPER

View Article Online
View Journal | View Issue

Cite this: *RSC Adv.*, 2021, **11**, 36577

Effects of mesoporous silica particle size and pore structure on the performance of polymer-mesoporous silica mixed matrix membranes†

Junhui Wang,[a] Gang Wang,[b] Zhongshen Zhang,*[c] Gangfeng Ouyang[ade] and Zhengping Hao*[c]

The fabrication of mixed matrix membranes (MMMs) has been regarded as an effective and economic approach to enhance the gas permeability and selectivity properties of conventional polymeric membranes for gas separation applications. However, the poor compatibility between polymeric matrix and inorganic filler in MMMs could lead to the generation of interfacial defects resulting in reduced gas selectivity. In this work, with the aim of studying the effect of particle size and pore structure of the filler on the performance of the resultant MMMs, nano/micro sized spherical mesoporous silicas with 2D/3D pore structure (MCM-41 and MCM-48) were synthesized and selected as fillers for the preparation of polydimethylsiloxane (PDMS)-based MMMs. The separation properties of the membranes prepared were characterized by permeability measurements for nitrogen and organic vapors (C_3H_6 and n-C_4H_{10}). Compared with microsized particles, nanosized fillers have better dispersion in the polymer matrix which could minimize the formation of non-selective microvoids around the particles, leading to higher vapor/N_2 ideal selectivities of the MMMs, even at the high loading (15 wt%). Moreover, due to the conventional random packing orientation of the particles in the polymer, vapor permeation was severely hindered in the MMMs fabricated from mesoporous silica with 2D pore channels. The interface morphologies and gas diffusion paths in the MMMs have also been proposed. With an optimum loading of nanosized MCM-48 (3D pore structure), the vapor permeabilities and vapor/N_2 ideal selectivities of the MMMs were shown to increase simultaneously, compared with the neat polymer membrane.

Received 3rd July 2021
Accepted 31st October 2021

DOI: 10.1039/d1ra05125c

rsc.li/rsc-advances

1. Introduction

Organic compounds such as ethylene, propylene, and butane are important industrial raw materials. In petrochemical processes, the excess monomers would remain in the off-gas stream. If these monomers are emitted to the atmosphere, it would cause serious environmental problems, such as the formation of fine particles, photochemical smog and global warming. Therefore, it is necessary and important to recover the unreacted organic materials from the off-gas for reuse.[1,2]

The membrane separation method has a good application prospect in the field of gas separation, owing to its low price, desirable physical robustness and good processability.[3–5] However, polymeric membranes are suffered from the trade-off relationship between gas permeability and selectivity, and still do not meet the requirements of the current advanced membrane technology due to their low separation performance (moderate selectivity) both at lab and commercial scale.[3,6] An economic alternative approach to solve this problem is to combine the advantages of both polymers and inorganic fillers, fabricating the mixed matrix membranes (MMMs).[7–9] In recent years, different kinds of inorganic materials were employed as fillers to fabricate MMMs, such as zeolites, silicas, clays, activated carbons, carbon nanotubes, carbon molecular sieves, metal–organic frameworks (MOFs), *etc.*[10–16]

The most important factor influencing the MMM success is to obtain a good compatibility between the continuous (polymer) and disperse (filler) phase.[3] Apart from adjusting the surface chemical composition of the filler to minimize filler–polymer gaps, proper regulation of the particle size is also proved to be an effective approach to avoid non-selective defects

[a]*MOE Key Laboratory of Bioinorganic and Synthetic Chemistry/KLGHEI of Environment and Energy Chemistry, School of Chemistry, Sun Yat-Sen University, No. 135, Xingang Xi Road, Guangzhou, Guangdong, 510275, China*

[b]*School of Materials Design & Engineering, Beijing Institute of Fashion Technology, Beijing, 100029, China*

[c]*National Engineering Laboratory for VOCs Pollution Control Material & Technology, Research Center for Environmental Material and Pollution Control Technology, University of Chinese Academy of Sciences, Beijing, 101408, China. E-mail: zszhang@ucas.ac.cn; zphao@ucas.ac.cn*

[d]*Chemistry College, Center of Advanced Analysis and Gene Sequencing, Zhengzhou University, Kexue Avenue 100, Zhengzhou 450001, China*

[e]*Provincial Key Laboratory of Emergency Test for Dangerous Chemicals, Guangdong Provincial Engineering Research Center for Ambient Mass Spectrometry, Institute of Analysis, Guangdong Academy of Sciences (China National Analytical Center Guangzhou), 100 Xianlie Middle Road, Guangzhou 510070, China*

† Electronic supplementary information (ESI) available. See DOI: 10.1039/d1ra05125c

formation. Tantekin-Ersolmaz *et al.* investigated the effect of particle size on the performance of silicalite-PDMS mixed matrix membranes, and found that the gas permeability values decreased when relatively smaller particle sizes were employed, probably due to the enhanced area and number of zeolite–polymer interfaces that the gas molecules have to cross in these cases.[17] Suen *et al.* found that compared with lamellar Na-montmorillonite clay (mean length = 500 nm), the incorporation of 70 nm spherical TiO_2 particles into polyethersulfone (PES) could form an ideal interface morphology leaded to an increase of gas selectivity compared to the pure polymer membrane.[10] It has also been reported that nanosizing the particle size of MOF could enhance its dispersion within the polymer matrix to minimize non-selective microvoid formation around the particles.[11] However, on the contrary, Coronas *et al.* stated that compared with the nanosized particles (MCM-41), 2–4 μm particles (MCM-48) could provide a lower external surface area and minimize the agglomeration, hence improving dispersibility and interaction with the polymer.[4]

These inconsistent conclusions made by the above literatures could be attributed to the application of different kinds of inorganic particles for comparison, since the pore size and pore channel orientation of the inorganic fillers are of great importance for the performance of MMMs. According to the Maxwell equation, an increase in the amount of less permeable dispersed phase in the polymer matrix decreases the permeability.[18] Therefore, the addition of microporous fillers (such as zeolites) usually decreases the gas permeability of MMMs, and conversely, the addition of large pore fillers would increase the gas permeability.[4,12,17,18] Moreover, it has been demonstrated that the gas permeability can be significantly improved by aligning the pore orientation parallel to the gas diffusion path, by creating more available nanoporosity in the polymers having good permeation potential.[12,16] Therefore, textural properties (pore size and structure) and particle size distributions should be taken into account as the critical variables to obtain a high-performance MMM.

Since the discovery of the M41S family in 1992 by Kresge *et al.*, a variety of ordered mesoporous materials have been synthesized with various framework compositions, morphologies and pore structures.[19–22] The particle shape, size and pore structure could be easily manipulated by adjusting surfactants and structure-directing agents, which makes these materials (*e.g.*, MCM-41 and MCM-48) promising for the development of a new generation of MMMs and suitable for investigating the effects of factors that influence the performance of MMMs.[4,14,23] Moreover, mesoporous materials possess pores with sizes ranging from 2 nm to 50 nm, which allow the penetration of the polymer chains (most of the cross-section areas per chain are around 1 nm).[24,25] Such good contact could lead to better wetting and dispersion of particles, thus suppressing the formation of voids at the interface and improving the separation performance of the MCM-48/PS MMMs.[4]

In this study, in order to investigate the effects of particle size and pore structure on the performance of mesoporous silica-PDMS mixed matrix membranes, three kinds of mesoporous silicas (nm MCM-48, nm MCM-41 and μm MCM-48) with the same pore diameter, but different particle size (nano and micro) and pore structure (2D and 3D) were elaborately synthesized and employed as fillers. The MCM mesoporous silicas were characterized by X-ray diffraction (XRD), pore size analysis, and high resolution-transmission electron microscope (HR-TEM). A series of MMMs with different type and various dosage of MCM were fabricated. Characterization and gas permeation measurements show that the particle size and pore structure of fillers significantly influenced the performance of matrix membranes. Based on these research results, the interface morphologies and possible gas diffusion paths in different MCM/PDMS MMMs were proposed.

2. Experimental section

2.1 Preparation of mesoporous silica particles

2.1.1 Preparation of nm MCM-48. nm MCM-48 mesoporous silica nanoparticles (MSNs) were synthesized based on the modified Stöber method, using a mixture of cetyltrimethylammonium bromide (CTAB) and ethanol as structure-directing agents. Tetraethoxysilane (TEOS) and triblock copolymer F127 ($EO_{106}PO_{70}EO_{106}$) were applied as a silica source and a particle dispersion agent respectively.[26] In a typical synthesis, 0.87 g of CTAB and 5.89 g of F127 were dissolved in a mixture of 180 mL of distilled water, 59.7 g of ethanol and 5.1 g of 28 wt% ammonium hydroxide solution at room temperature (RT). After complete dissolution, 3.12 g of TEOS was added into the above mixture at once. After mechanical stirring at 1000 rpm for 1 min, the solution was kept at static condition for 24 h at RT for silica condensation. The white solid product was recovered by ultrahigh speed centrifuge, washed with water and dried at 70 °C. The template was removed by calcination at 550 °C for 5 h with a heating rate of 5 °C min^{-1}.

2.1.2 Preparation of nm MCM-41. nm MCM-41 MSNs were prepared by a surfactant-templated, base-catalyzed condensation procedure as reported by Shi.[27] 1.02 g of CTAB was dissolved in 480 mL of distilled water and 3.5 mL of sodium hydroxide solution (2 M), and then the mixture was heated at 80 °C under vigorous stirring. After then, 5.0 mL of TEOS was added dropwise to the reaction mixture. The temperature was kept at 80 °C for 2 h, after which the resulting white solid was filtered, washed with abundant methanol and water, and dried under vacuum overnight. The template was removed by extraction in an ethanol–HCl mixture for 12 h, followed by calcination at 550 °C for 4 h with a heating rate of 5 °C min^{-1}.

2.1.3 Preparation of μm MCM-48. μm MCM-48 mesoporous silica particles were synthesized by a facile method at room temperature.[28] Under vigorous stirring, 1.2 g of CTAB was added into 50 mL of deionized water. After completely dissolved, 25 mL of ethanol was poured into the clear solution. After then, 6 mL of aqueous NH_3 was added to the surfactant solution and 1.8 mL of TEOS was added immediately. After stirring at 300 rpm for 4 h, the powder was recovered by filtration, washed with water and dried at 80 °C overnight. The dried powder was then grounded and calcined at 550 °C for 6 h with a heating rate of 3 °C min^{-1} to remove the template.

2.2 Preparation of pure PDMS and mesoporous silica-PDMS MMMs

The membranes were prepared by a solvent casting method. Dense, unfilled films of PDMS were made from Momentive RTV 615 A/B

(Wenhao Chip Technology, China) composed of two components: component A contains platinum catalyst while component B contains the cross-linker. After optimization, components A and B were mixed at 10 : 1 (w/w) ratio in heptane to make a final PDMS concentration of 60 wt%. After stirring for 1 h and ultrasonic treatment for 30 min, the polymer solution was cast onto the PVDF membrane to form the composite membrane. The prepared membranes were placed in oven at 45 °C for 48 h and then cured for 3 h at 100 °C. The basement PVDF membranes were immersed in deionized water at room temperature for 3 days and then thermally treated at 120 °C for 12 min before use.

Before MMM preparation, the mesoporous silica powders were dried at 80 °C overnight. Certain amount (2–15 wt%, with respect to PDMS content) of silica powders were added to heptane and then dispersed through stirring for 30 min. After then, the PDMS components were added to the dispersion to obtain a 60 wt% polymer solution. The mixture was further stirred for 1 h and sonicated for 30 min, and then prepared similarly to that of the pure PDMS membranes.

2.3 Physico-chemical characterization

The textual properties of the mesoporous silica particles were investigated by nitrogen adsorption and desorption at 77 K using a volumetric adsorption analyzer (ASAP2020, Micromeritics Instrument Corporation, USA). The BET (Brunauer–Emmett–Teller) surface areas were calculated from N_2 adsorption isotherms within the relative pressure ranging from 0.05 to 0.25. The pore size distributions were obtained from the N_2 desorption isotherms using the BJH method. The ordered mesopore regularity of the samples was characterized by X-ray diffractometer (X'Pert PRO MPD, Panalytical, the Netherlands) with Cu Kα radiation ($\lambda = 0.1541$ nm) at 40 kV and 40 mA. The morphologies of membranes and mesoporous silica particles were inspected using scanning electron microscopy (SEM, S-3000N, Hitachi, Japan) and transmission electron microscopy (TEM, H-7500, Hitachi, Japan). The pore structures of the mesoporous silica were inspected using the high resolution-TEM on a JEM 2010 at 200 kV. The glass transition temperature (T_g) of the membranes was measured on a SEIKO DSC 6220. About 10 mg of each sample was placed in an aluminum pan and the measurements were carried out from −160 °C to −50 °C at a 10 °C min^{-1} ramping rate under a N_2 atmosphere. Sorption studies were investigated using an Intelligent Gravimetric Analyzer (IGA-002, Hiden Isochema Ltd, UK). The apparatus has an ultrahigh vacuum system comprising a microbalance, temperature regulation and pressure control system, all of which are fully computerized. The adsorption and desorption isotherms were determined by the approach of monitoring equilibrium in real time using a computer algorithm.[29] For each measurement, the samples were outgassed to a constant weight, at <10^{-6} Pa, at 100 °C.

2.4 Gas separation measurements

Pure gas separation (N_2, C_3H_6, n-C_4H_{10}) of the membranes were measured at 35 °C using a custom-built membrane module as reported in our previous work.[29] The gas permeability was calculated using the following equation in the steady state:[30]

$$P = \frac{Nl}{(p_f - p_p)A}$$

where N is the permeate flow (cm^3 s^{-1}), l is the membrane thickness (cm), A is the membrane area (cm^2), p_f and p_p are the feed and permeate pressure in 1.333224 × 10^3 Pa (cmHg), respectively. The permeability is expressed in Barrer (1 Barrer = 10^{-10} cm^3 (STP) cm cm^{-2} s^{-1} cmHg^{-1}).

The ideal selectivity of a membrane is the ratio of the permeabilities of pure gas components A and B:

$$\alpha_{A/B} = \frac{P_A}{P_B}$$

Mixed-gas permeation properties of membranes were determined with feed mixture a feed mixture containing 25 vol% C_3H_6 and 75 vol% N_2. The pressure difference over the membrane was 0.5 bar, the permeation side was kept at atmospheric pressure. The composition of the permeate stream was determined with a gas chromatograph (7890A, Agilent). The total permeate flow was measured with a digital flowmeter. The permeability of each component can be calculated with the following expression:

$$P_i = \frac{N_i l}{\Delta p_i A}$$

where P_i and N_i represent the permeability (Barrer) and volumetric flow rate (cm^3 s^{-1}) of gas "i", respectively; Δp_i denotes the pressure difference (cmHg) between two side of the membrane.

3. Results and discussion

3.1 Characterization of mesoporous silica particles

3.1.1 Small-angle X-ray diffraction analysis. The XRD analysis was employed to determine the crystalline structure of the mesoporous silica particles and the results are shown in

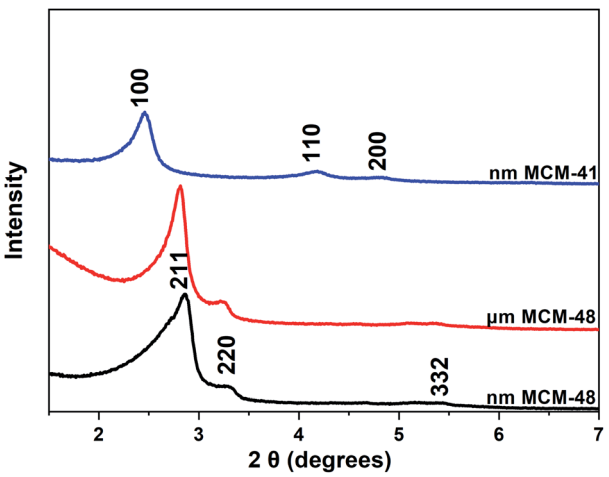

Fig. 1 XRD patterns of nm MCM-48, nm MCM-41 and μm MCM-48 mesoporous silica particles.

Fig. 1 and Table S1.† The nm MCM-41 sample exhibits three well-defined peaks, with d values of 3.67, 2.14, 1.83 nm, which can be indexed as (100), (110) and (200) reflections, confirming its 2D hexagonal ordered mesopores ($p6m$).[27] For nm MCM-48 and μm MCM-48, the peaks of (211), (220) and (332) diffractions reflect the formation of 3D cubic $Ia3d$ structures.[26] In order to synthesize mesoporous silicas with spherical morphologies, lower temperatures were applied without hydrothermal treatment, which leads to decreases in d-spacing compared with those without deliberate morphology control in the ref. 19 and 31. This might be an indication of the formation of low-quality mesostructures.[26] Moreover, compared with μm MCM-48, broadening of the diffraction peaks for nm MCM-48 can be observed, mainly due to a decrease in the reflection domains of mesophase from the decrease of spherical silica nanoparticle size,[26] which could also be observed in the sample of nm MCM-41.

3.1.2 N_2 adsorption–desorption. Shown in Fig. 2a and b are the nitrogen adsorption–desorption isotherms and the corresponding pore size distributions of mesoporous silicas, respectively. In Fig. 2a, it could be observed that all of the adsorption isotherms are of type-IV (IUPAC classification),[32] and marked inflections are perceived between the relative pressures (p/p_0) of 0.2 and 0.4. This is caused by capillary condensation during the adsorption step and is an indication of the mesoporosity of the samples.[28,33] Moreover, for nm MCM-48 and nm MCM-41, there exists another capillary condensation step in the relative pressure above 0.9 in the adsorption branch, due to the interparticle voids, which could indirectly reflect the size of particles, since smaller particle size always show higher step.[27] In addition, the capillary condensation and evaporation are nearly reversible owing to their relatively small mesopore size (<3 nm, Fig. 2b). The pore sizes of both MCM-48 samples are around 2.06 nm, and that for MCM-41 is near 2.6 nm, which are all large enough for the gas diffusion. As shown in the table inserted in Fig. 2b, nm MCM-48 and nm MCM-41 both exhibit much higher BET surface areas, compared with that of μm MCM-48. Moreover, the smaller particle sizes of nm MCM-48 and nm MCM-41 result in the generation of abundant interparticle voids, thereby increasing the external surface areas, which might be beneficial to the effective attachment with PDMS polymer chains.

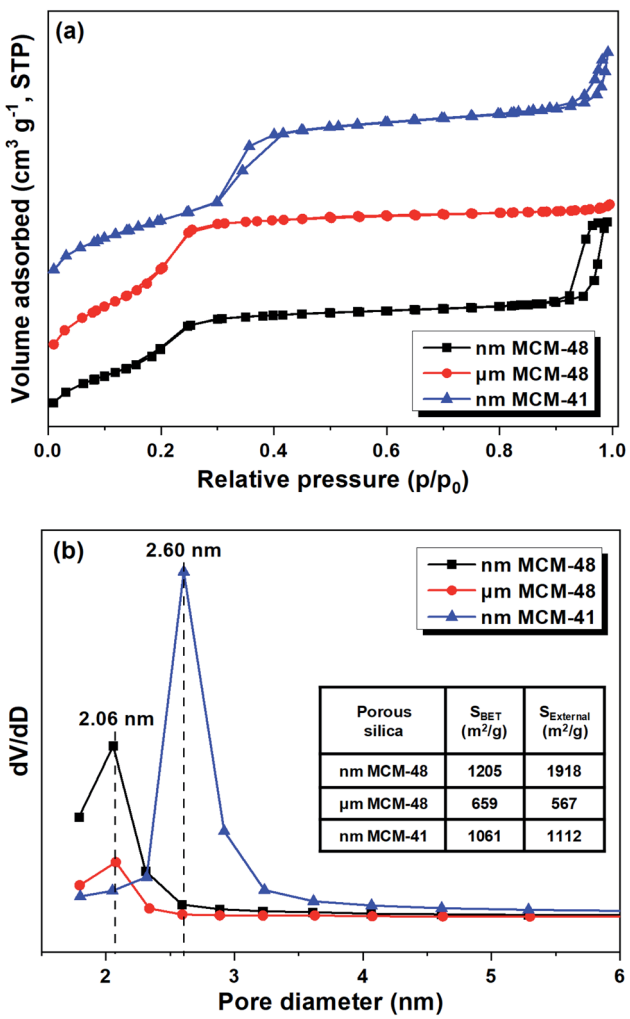

Fig. 2 (a) Nitrogen adsorption–desorption isotherms of the mesoporous silica particles; (b) BJH pore size distributions and textual properties (table insert).

3.1.3 TEM characterization. The TEM images (Fig. 3) show that the spherical nm MCM-48 and nm MCM-41 have an uniform diameter of ~100 nm. In contrast, the spherical μm MCM-48 showed an average diameter of ~1 μm. Besides, the cubic mesostructures ($Ia3d$) of nm MCM-48 and μm MCM-48 are confirmed by the HR-TEM images, recorded along [100] and [111], respectively.[34] Similarly, nm MCM-41 show hexagonal array of cylindrical mesopores and ordered 2D channels (~2.5 nm in diameter) along the [100] direction as exhibited in Fig. 3d.

3.2 Characterization of the mixed matrix membranes

3.2.1 SEM analysis. To investigate the dispersion of the mesoporous silicas within the polymer matrix, cross-sectional micrographs of the MMMs were examined by SEM (Fig. 4). The cross-sections of these membranes show the common asymmetric structure consisting of a dense PDMS layer on the surface of the PVDF supports with no gaps between them. Moreover, the morphologies of the PDMS layers remain dense and flat upon addition of fillers in the matrix. For all the 2 wt% MCM/PDMS MMMs (Fig. 4b–d), the nano/micro-particle distribution is apparently homogeneous without agglomeration. Even in the SEM photos with high magnification (inserted in Fig. 4b–d), good dispersion of the filler particles throughout the polymer matrix could also be observed. For the 10 wt% and 15 wt% nm MCM-48/PDMS MMMs (Fig. 4e and f), the particles were agglomerated to some extent in the PDMS matrix. However, from the microscopic view (as shown in images inserted in Fig. 4e and f), no micro-sized voids could be observed.

3.2.2 Glass transition temperature. The increases in glass transition temperature (T_g) of MMMs by the incorporation of fillers could be considered as an indication of increased chain rigidity due to the interactions between polymer matrix and

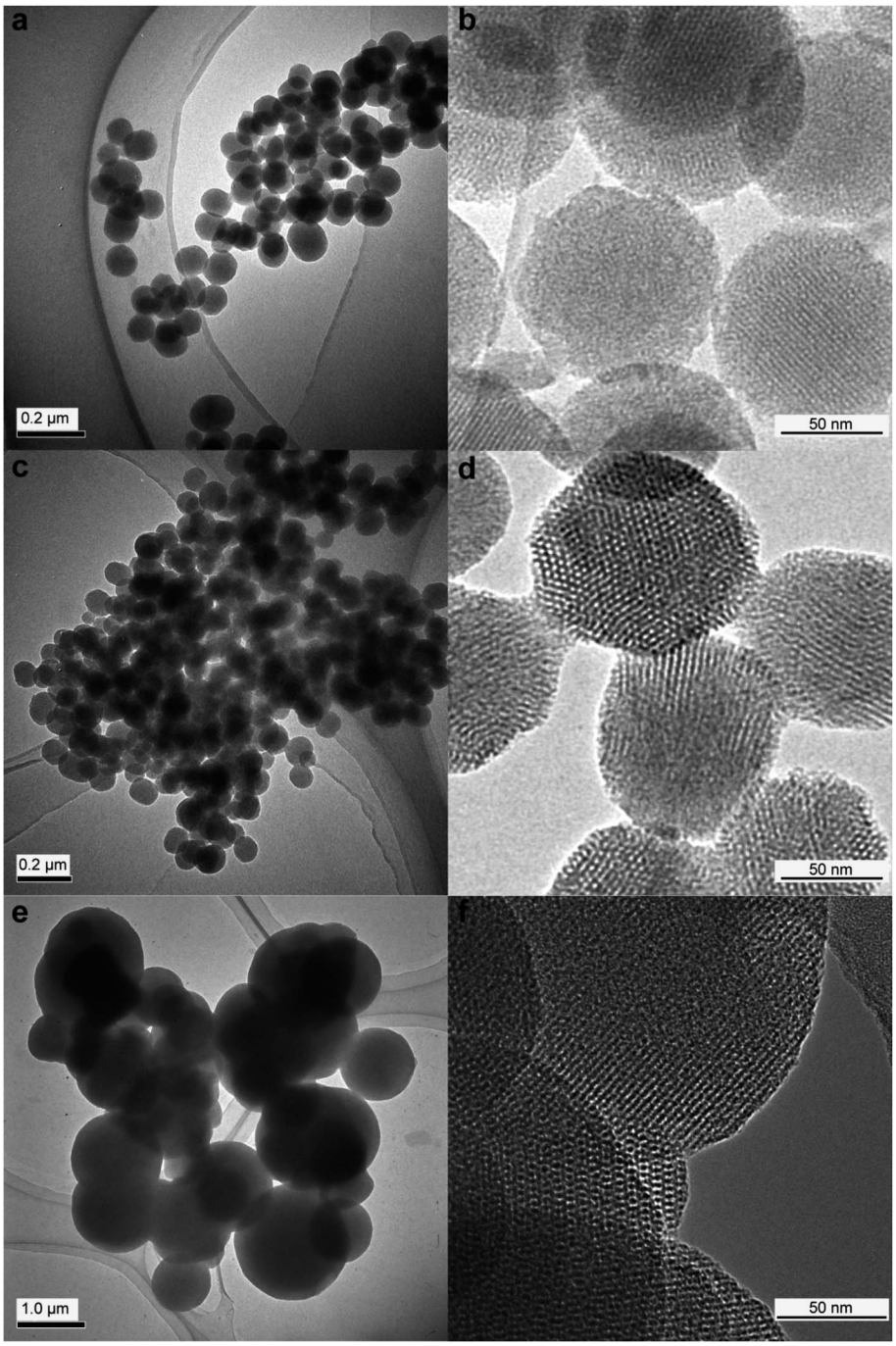

Fig. 3 TEM and the relative HR-TEM images of nm MCM-48 (a and b), nm MCM-41 (c and d) and μm MCM-48 (e and f).

filler particles.[35,36] The T_g of the MMMs prepared in this work are presented in Fig. S2.† It can be observed that the addition of micro-sized MCM has little effect on the T_g, indicating the negligible interaction between the MCM and polymer phase. In sharp contrast, the addition of nano-sized MCM could increase the T_g of MMMs remarkably, which indicates increased interaction between the nano-sized MCM and PDMS.

3.2.3 Gas separation measurements. The effects of filler particle size on the performance of matrix membranes were investigated by introducing fillers with different particle sizes. The separation properties of the membranes were characterized by permeability measurements for N_2 and organic vapors (C_3H_6 and n-C_4H_{10}) (Fig. 5 and 6). Compared with the pure PDMS membrane, the addition of nanosized MCM-48 induced the decrease of N_2 permeability, while the micro-sized MCM-48 conversely gave rise to large increase of N_2 permeability. The addition of nanosized MCM-48 can induce the rigidification of the PDMS polymer chains, as evidenced by the increased T_g (Fig. S2†). Rigidification of the PDMS could lead to the inhibition of polymer chain mobility and reduce the free volume for

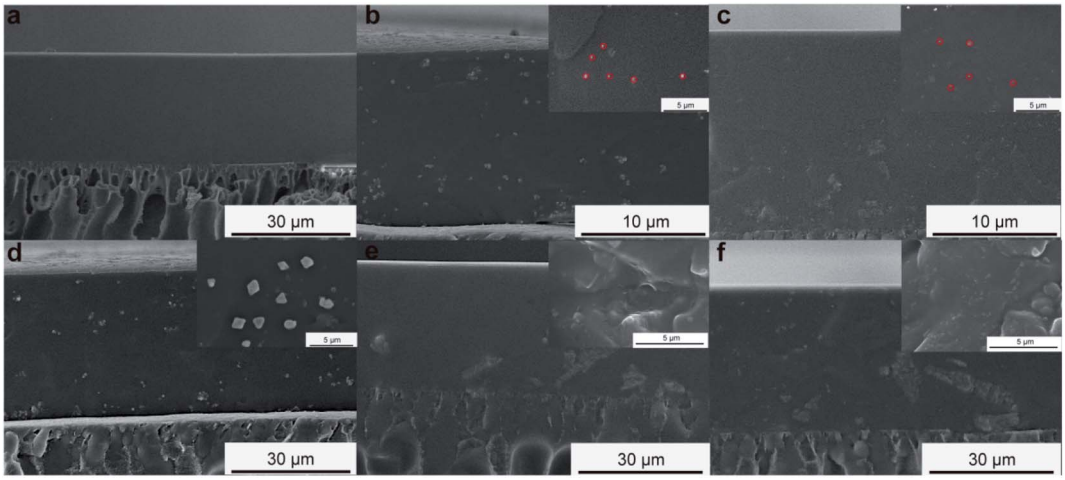

Fig. 4 Cross-sectional SEM images of (a) pure membrane, (b) 2 wt% nm MCM-48/PDMS MMM, (c) 2 wt% nm MCM-41/PDMS MMM, (d) 2 wt% μm MCM-48/PDMS MMM, (e) 10 wt% nm MCM-48/PDMS MMM and (f) 15 wt% nm MCM-48/PDMS MMM (inserted in b–f are the SEM photos with large magnification).

diffusion, thereby decreasing the N_2 permeability. As for the organic vapors, at the same loadings of both nm MCM-48 and μm MCM-48 (2 wt%), increases in C_3H_6/n-C_4H_{10} permeabilities were observed (Fig. 6a and c). However, the ideal selectivities of C_3H_6/N_2 and n-C_4H_{10}/N_2 are very different. For 2 wt% nm MCM-48 MMM the ideal selectivities were shown to increase by 102% and 47%, respectively, while those of 2 wt% μm MCM-48 MMM were shown to decrease by 42% and 59%, respectively, compared with the neat polymer membrane. The lower N_2 permeability and higher ideal selectivities of 2 wt% nm MCM-48 MMM can be attributed to the good conformability between the interface of filler and polymer, as evidenced by the increased T_g, which effectively avoided the formation of voids and defects.[37–39]

For low nm MCM-48 additions, there is an increase for selectivity meanwhile there is no loss in overall permeability.

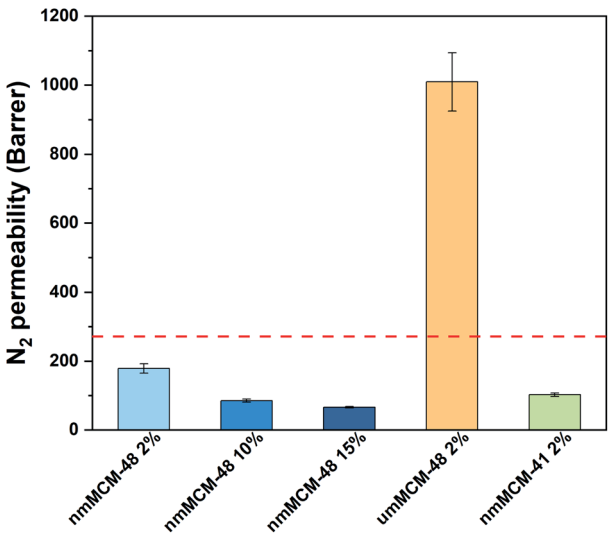

Fig. 5 N_2 permeability of different MCM/PDMS MMMs at 0.5 bar at 35 °C (the permeability of pure PDMS membrane is indicated by the red dashed line).

Generally, rigidification of the polymer leads to increased selectivity, but also always leads to low permeability.[11] This anomaly is due to that the MCM-48 itself is a large-pore system that compensates for the loss in PDMS permeability in the composite. According to the solution-diffusion model,[40] the transport of gases in polymer membranes are governed by two factors: sorption and diffusion. While the diffusion step favors small molecules, the sorption step favors large and condensable molecules. Gas permeability and selectivity in rubbery membrane (PDMS) is more strongly influenced by the solubility factor than diffusivity factor. Vapors with condensability could cause increased polymer chain mobility and plasticization,[41] therefore dissolving the rigidified polymer chains and diffusing into the pores of nm MCM-48, in which the diffusion rate could be greatly enhanced. This is why MMM with 2 wt% nanosized MCM-48 can increase the permeabilities of vapors. It should be mentioned that there is a decrease in the membrane permeability as more nm MCM-48 is added to the polymer. This is attributed to the formation of more rigidified layers and the collection of the nanosized fillers into an essentially non-porous aggregate.[11] Even for the inclusion of 15 wt% filler, the use of nm MCM-48 particles created less voids and defects on the MMM (as shown in Fig. 4f) such that its vapors/N_2 selectivities are still satisfactory. In sharp contrast, with the increased loading of μm MCM-48, the MMMs exhibited enhanced N_2 permeability and reduction of ideal selectivities (Fig. S3†). This could be attributed to the non-selective diffusion at a defective interface (voids and defects) between micro-particles and polymer, as observed in the SEM images (Fig. S4†). Therefore, it can be revealed that compared with micro-sized particles, nanosized fillers could improve the interaction between polymer and filler and avoid the formation of non-selective defects.

The effect of pore structure of fillers on the performance of MMMs was explored by employing fillers with 3D and 2D pore structure, respectively. Both nm MCM-48 and nm MCM-41 are spherical particles with uniform diameter of ~100 nm (Fig. 3),

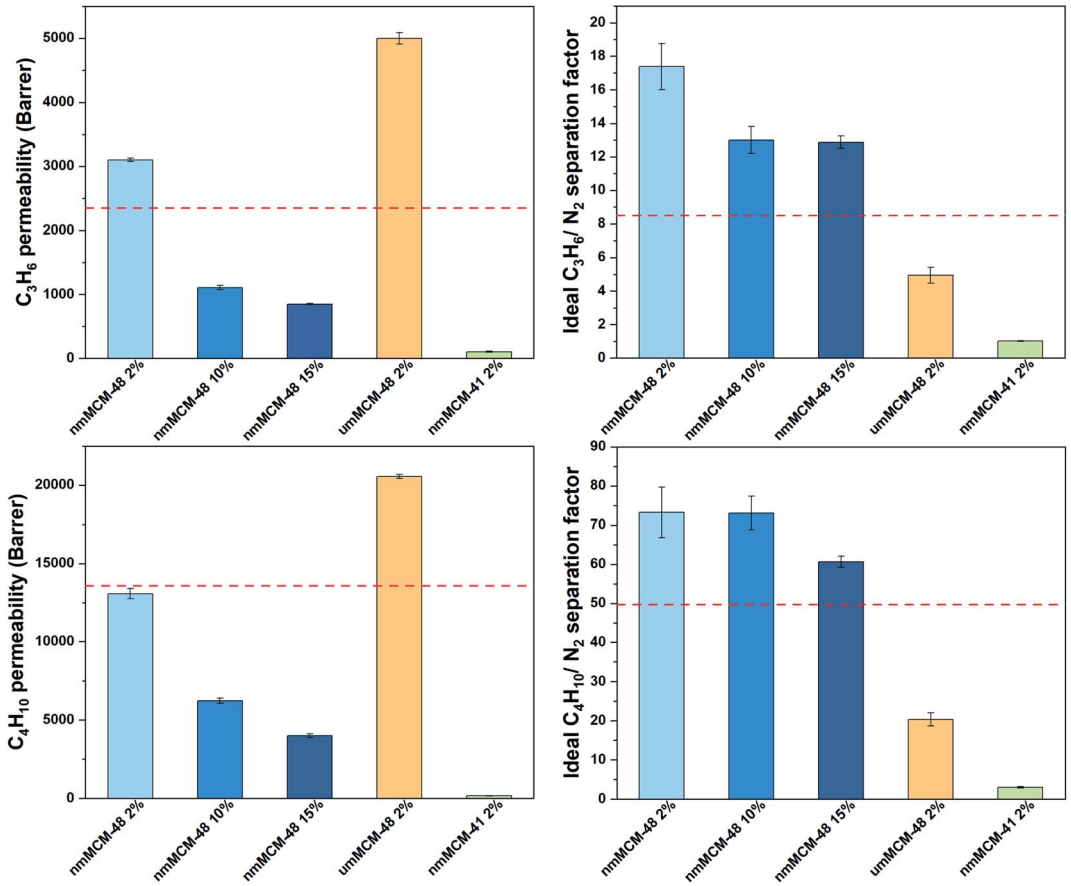

Fig. 6 C_3H_6 and n-C_4H_{10} permeability and n-C_4H_{10}/N_2, C_3H_6/N_2 ideal selectivity of different MCM/PDMS MMMs at 0.5 bar at 35 °C (the relative permeability and ideal selectivity of pure PDMS membrane is indicated by the red dashed line).

but with different pore structures: the former possesses three-dimensional (3D) bicontinuous cubic arrangement of mesopores, while the latter has two-dimensional (2D) hexagonal array of cylindrical mesopores which is not interconnected (Fig. 2 and 3). As shown in Fig. 6a, the incorporation of nm MCM-41 also induces the decrease of N_2 permeability, which further proves the better wetting and dispersion of nanosized particles in the polymer matrix.[11] However, in sharp contrast to nm MCM-48, drastic declines of C_3H_6/n-C_4H_{10} permeabilities (decrease by 95%/98% to the neat polymer membrane), and C_3H_6/N_2 and n-C_4H_{10}/N_2 ideal selectivities (decrease by 88% and 94%) were observed, when the same loading of nm MCM-41 was added. As proposed in our previous report,[29] the large mesopores of the fillers could provide channels with much faster diffusion rates for organic vapors, when they dissolve the rigidified polymer chains at the pore entrance and enter into the pores of the mesoporous silicas. This is why the incorporation of nm MCM-48 could increase the vapor permeabilities and vapor/N_2 selectivities simultaneously. The poor performance of nm MCM-41 might be due to its 2D pore structure. As we know, the fillers disperse in the polymer matrix randomly, and most of the pore orientations cannot be parallel to the gas diffusion path, which will severely hinder the diffusion of the gases.

In order to prove the above assumptions, gas diffusions in different MMMs were investigated by measuring the gravimetric sorption isotherms. It should be noted that the isotherms for N_2 cannot be obtained because there is no interaction between the membranes and N_2. The adsorption amounts of C_3H_6 in MCM/PDMS MMMs and mesoporous silicas at 0.5 bar at 35 °C are

Table 1 Calculated and experimental adsorption amount of C_3H_6 in MCM/PDMS MMMs at 0.5 bar at 35 °C

	Amount adsorbed (mmol g^{-1})			
Membrane	Experimental value	Calculated value	Mesoporous silica	Amount adsorbed (mmol g^{-1})
Pure PDMS	0.042	—		
2 wt% nm MCM-48 MMM	0.057	0.058	nm MCM-48	0.89
2 wt% μm MCM-48 MMM	0.073	0.067	μm MCM-48	1.34
2 wt% nm MCM-41 MMM	0.046	0.051	nm MCM-41	0.51

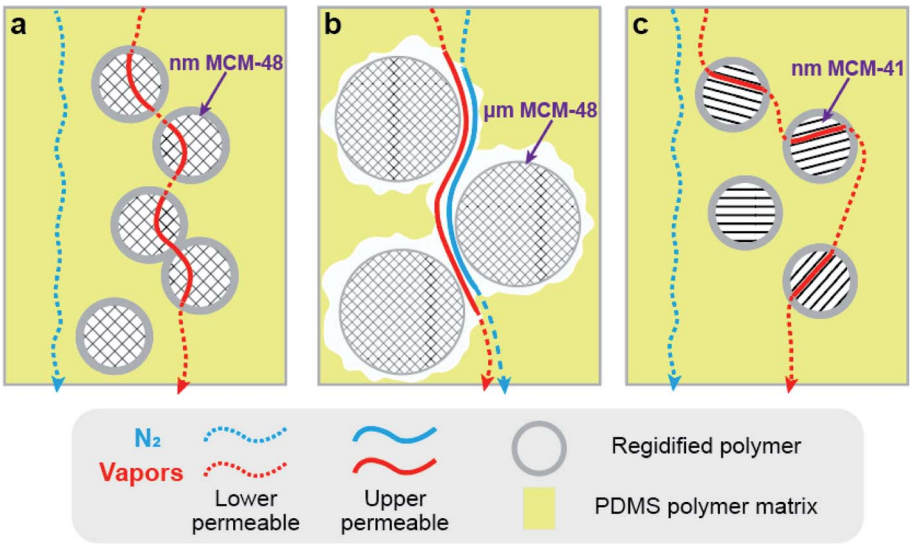

Fig. 7 Hypotheses for the interface morphologies and gas diffusion pathways through nm MCM-48/PDMS MMM (a), μm MCM-48/PDMS MMM (b) and nm MCM-41/PDMS MMM (c).

listed in Table 1. It can be observed that C_3H_6 adsorption amounts of all the MCM/PDMS MMMs are higher than that of the pure polymer membrane, indicating that the vapor could diffuse into the pores of the silicas. The experimental adsorption amount of 2 wt% nm MCM-48 MMM is nearly the same as the calculated value, which means the vapor could diffuse to all the channels of the filler and no voids formed on the filler–polymer interface. However, for the 2 wt% μm MCM-48 MMM, the experimental value is larger than the theoretical one, implying the formation of extra nano/micro sized voids in which vapors adsorb and condense. Conversely, compared to the calculated value, the experimental one decreases, for 2 wt% nm MCM-41 MMM, revealing that vapors could only penetrate to partial portion of the pores in nm MCM-41, consistent with the gas separation performance.

3.2.4 Interface morphology hypothesis. The nanoscale morphology of the filler–polymer interface is a critical determinant of the gas transport properties of organic/inorganic MMMs. According to the gas separation/sorption performances and the morphology hypothesis raised by our previous work,[29] the interface morphologies between the mesoporous silicas and the PDMS polymer have been proposed.

As shown in Fig. 7a, nm MCM-48 well disperse in the polymer matrix, and the rigidified layers form at the filler–polymer interface, possibly due to the partial pore blocking of MCM-48 by the polymer chains.[4,42,43] According to the solution–diffusion model, vapors with condensability could cause increased polymer chain mobility and plasticization, therefore dissolving the rigidified polymer chains and diffusing into the pores of nm MCM-48. And once the vapors enter into the pores with large diameter, the diffusion rates could be increased dramatically. In contrast, N_2 is inert and noncondensable, and as a result, it cannot pass through the rigidified polymer layer and utilize the pores of nm MCM-48. The increased tortuosity caused by the fillers leads to reduced permeability of N_2. Therefore, the vapor permeabilities and vapor/N_2 ideal selectivities could be increased at the same time for 2 wt% nm MCM MMMs.

For the μm MCM-48 MMM (Fig. 7b), because of the large particle size, the fillers could not be wrapped perfectly by the polymer chains, leading to the formation of voids and defects. Both N_2 and vapors prefer to diffuse through these non-selective voids, resulting in higher permeabilities and lower selectivities. In the nm MCM-41 MMM (Fig. 7c), it could not be guaranteed that the 2D pores are parallel to the gas diffusion path. As a result, even though vapors could diffuse into the pores, the increases in the diffusion path lengths experiencing when they traverse the membrane lead to decreased permeabilities. At the meantime, due to the acceleration effect of the pores of nm MCM-41, the values of the vapor/N_2 ideal selectivities are still higher than one.

3.2.5 Mixed gas separation performance and stability of nm MCM-48/PDMS MMMs. As shown in Fig. S5a,† the MMMs show lower C_3H_6 permeabilities in mixed gas over the pure gas. The less fraction of C_3H_6 in the mixed gas leads to lower solubility in PDMS matrix, thus resulting in decreased transport in the MMMs. As illustrated in Fig. S5b,† the C_3H_6/N_2 selectivity of gas mixture is also lower than that of pure gas. This could be ascribed to the decline of C_3H_6 permeability and increase of N_2 permeability in gas mixture, which in turn cause the reduction of selectivity. Fig. S6† presents the stability of the 2 wt% nm MCM-48 MMM tested by a gas mixture at 0.5 bar and 35 °C. MMM exhibited the average gas separation properties (C_3H_6 permeability: 2653 Barrer; C_3H_6/N_2 selectivity: 12.96), which changed slightly for 120 h, indicating the good stability of the nm MCM-48/PDMS MMM.

4. Conclusions

In this work, several kinds of MMMs fabricated with nano/micro sized mesoporous silicas with 2D/3D pore structure

(MCM-41 and MCM-48) and PDMS were prepared and employed to study the effect of the particle size and pore structure of the filler on the gas separation performances of the resultant MMMs. As for the effect of particle size, nanosized fillers could have better compatibility with the polymer matrix, and no non-selective defects formed at the filler–polymer interface. As a result, the MMMs achieved enhanced vapor/N_2 ideal selectivities, even at higher loading (15 wt%), compared with those of the neat polymer membrane. As regards the pore structure, due to the conventional random packing orientation of the particles in the polymer, gas permeation could be severely hindered in the MMMs fabricated from mesoporous silica with 2D pore channels. Assisted by the sorption data of mesoporous silicas, pure membrane and MMMs, the interface morphologies and gas diffusion paths in the MMMs have also been proposed. With an optimum loading of nanosized MCM-48 (3D pore structure), the vapor permeabilities and vapor/N_2 ideal selectivities of the MMM were shown to increase simultaneously due to the interconnected pore channels in the filler and the good filler–polymer interaction. This work would provide guidance on the rational design of MMMs with high performance.

Author contributions

J. W., Z. H. and Z. Z. conceived the project. J. W., G. W. and Z. Z. designed, analyzed, and discussed the experimental results. J. W. and G. W. performed the measurements. Z. H., Z. Z. and O. G. gave suggestions on the experiments and drafted the manuscript.

Conflicts of interest

There are no conflicts to declare.

Acknowledgements

We acknowledge financial support from the projects of the R&D Program of Beijing Municipal Education Commission (KJZD20191443001), the National Natural Science Foundation (Nos. 21806192, 22036003, 21737006 and 22076222), the Science and Technology Program of Guangzhou (202102021203), the Natural Science Foundation of Guangdong Province (2018A030313441), Guangdong Provincial Key R&D Programme (2020B1111350002), the Fundamental Research Funds for the Central Universities (19lgpy135) and Jiangsu Key Laboratory of Vehicle Emissions Control (OVEC053).

References

1 R. W. Baker, J. G. Wijmans and J. H. Kaschemekat, The design of membrane vapor–gas separation systems, *J. Membr. Sci.*, 1998, **151**, 55–62.
2 R. W. Baker and M. Jacobs, Improve monomer recovery from polyolefin resin degassing, *Hydrocarbon Process.*, 1996, **75**, 49–51.
3 J. Gascon, F. Kapteijn, B. Zornoza, V. Sebastián, C. Casado and J. Coronas, Practical approach to zeolitic membranes and coatings: state of the art, opportunities, barriers, and future perspectives, *Chem. Mater.*, 2012, **24**, 2829–2844.
4 B. Zornoza, S. Irusta, C. Tellez and J. Coronas, Mesoporous silica sphere-polysulfone mixed matrix membranes for gas separation, *Langmuir*, 2009, **25**, 5903–5909.
5 P. Bernardo, E. Drioli and G. Golemme, Membrane gas separation: a review/state of the art, *Ind. Eng. Chem. Res.*, 2009, **48**, 4638–4663.
6 L. M. Robeson, The upper bound revisited, *J. Membr. Sci.*, 2008, **320**, 390–400.
7 H. Zou, S. S. Wu and J. Shen, Polymer/silica nanocomposites: preparation, characterization, properties, and applications, *Chem. Rev.*, 2008, **108**, 3893–3957.
8 Y. Kudo, H. Mikami, M. Tanaka, T. Isaji, K. Odaka, M. Yamato and H. Kawakami, Mixed matrix membranes comprising a polymer of intrinsic microporosity loaded with surface-modified non-porous pearl-necklace nanoparticles, *J. Membr. Sci.*, 2020, **597**, 117627.
9 Y. Lu, H. Zhang, J. Y. Chan, R. Ou, H. Zhu, M. Forsyth, E. M. Marijanovic, C. M. Doherty, P. J. Marriott, M. M. B. Holl and H. Wang, Homochiral MOF–polymer mixed matrix membranes for efficient separation of chiral molecules, *Angew. Chem., Int. Ed.*, 2019, **58**, 16928–16935.
10 C.-Y. Liang, P. Uchytil, R. Petrychkovych, Y.-C. Lai, K. Friess, M. Sipek, M. Mohan Reddy and S.-Y. Suen, A comparison on gas separation between PES (polyethersulfone)/MMT (Na-montmorillonite) and PES/TiO_2 mixed matrix membranes, *Sep. Purif. Technol.*, 2012, **92**, 57–63.
11 B. Ghalei, K. Sakurai, Y. Kinoshita, K. Wakimoto, A. P. Isfahani, Q. Song, K. Doitomi, S. Furukawa, H. Hirao, H. Kusuda, S. Kitagawa and E. Sivaniah, Enhanced selectivity in mixed matrix membranes for CO_2 capture through efficient dispersion of amine-functionalized MOF nanoparticles, *Nat. Energy*, 2017, **2**, 17086.
12 G. Dong, H. Li and V. Chen, Challenges and opportunities for mixed-matrix membranes for gas separation, *J. Mater. Chem. A*, 2013, **1**, 4610–4630.
13 A. F. Bushell, M. P. Attfield, C. R. Mason, P. M. Budd, Y. Yampolskii, L. Starannikova, A. Rebrov, F. Bazzarelli, P. Bernardo, J. C. Jansen, M. Lanc, K. Friess, V. Shantarovich, V. Gustov and V. Isaeva, Gas permeation parameters of mixed matrix membranes based on the polymer of intrinsic microporosity PIM-1 and the zeolitic imidazolate framework ZIF-8, *J. Membr. Sci.*, 2013, **427**, 48–62.
14 S. Kim, E. Marand, J. Ida and V. V. Guliants, Polysulfone and mesoporous molecular sieve MCM-48 mixed matrix membranes for gas separation, *Chem. Mater.*, 2006, **18**, 1149–1155.
15 D. Vu, W. J. Koros and S. J. Miller, Effect of condensable impurity in CO_2/CH_4 gas feeds on performance of mixed matrix membranes using carbon molecular sieves, *J. Membr. Sci.*, 2003, **221**, 233–239.
16 A. Sharma, S. Kumar, B. Tripathi, M. Singh and Y. K. Vijay, Aligned CNT/Polymer nanocomposite membranes for hydrogen separation, *Int. J. Hydrogen Energy*, 2009, **34**, 3977–3982.

17 Ş. B. Tantekin-Ersolmaz, Ç. Atalay-Oral, M. Tatlıer, A. Erdem-Şenatalar, B. Schoeman and J. Sterte, Effect of zeolite particle size on the performance of polymer–zeolite mixed matrix membranes, *J. Membr. Sci.*, 2000, **175**, 285–288.

18 P. Gorgojo, S. Uriel, C. Tellez and J. Coronas, Development of mixed matrix membranes based on zeolite Nu-6(2) for gas separation, *Microporous Mesoporous Mater.*, 2008, **115**, 85–92.

19 C. T. Kresge, M. E. Leonowicz, W. J. Roth, J. C. Vartuli and J. S. Beck, Ordered mesoporous molecular-sieves synthesized by a liquid-crystal template mechanism, *Nature*, 1992, **359**, 710–712.

20 J. S. Beck, J. C. Vartuli, W. J. Roth, M. E. Leonowicz, C. T. Kresge, K. D. Schmitt, C. T. W. Chu, D. H. Olson and E. W. Sheppard, A new family of mesoporous molecular sieves prepared with liquid crystal templates, *J. Am. Chem. Soc.*, 1992, **114**, 10834–10843.

21 T. W. Kim, F. Kleitz, B. Paul and R. Ryoo, MCM-48-like large mesoporous silicas with tailored pore structure: facile synthesis domain in a ternary triblock copolymer–butanol–water system, *J. Am. Chem. Soc.*, 2005, **127**, 7601–7610.

22 Y. F. Lu, H. Y. Fan, A. Stump, T. L. Ward, T. Rieker and C. J. Brinker, Aerosol-assisted self-assembly of mesostructured spherical nanoparticles, *Nature*, 1999, **398**, 223–226.

23 K. Nocon-Szmajda, A. Wolinska-Grabczyk, A. Jankowski, U. Szeluga, M. Wojtowicz, J. Konieczkowska and A. Hercog, Gas transport properties of mixed matrix membranes based on thermally rearranged poly(hydroxyimide)s filled with inorganic porous particles, *Sep. Purif. Technol.*, 2020, **242**, 116778.

24 R. W. Baker, Future directions of membrane gas separation technology, *Ind. Eng. Chem. Res.*, 2002, **41**, 1393–1411.

25 R. L. M. Raymond and F. Boyer, Polymer chain stiffness parameter, σ, and cross-sectional area per chain, *Macromolecules*, 1977, **10**, 1167–1169.

26 T.-W. Kim, P.-W. Chung and V. S. Y. Lin, Facile synthesis of monodisperse spherical MCM-48 mesoporous silica nanoparticles with controlled particle size, *Chem. Mater.*, 2010, **22**, 5093–5104.

27 S. S. Jinlou Gu, Y. Li, Q. He, J. Zhong and J. Shi, Surface modification-complexation strategy for cisplatin loading in mesoporous nanoparticles, *J. Phys. Chem. Lett.*, 2010, **1**, 3446–3450.

28 R. Peng, D. Zhao, N. M. Dimitrijevic, T. Rajh and R. T. Koodali, Room temperature synthesis of Ti–MCM-48 and Ti–MCM-41 mesoporous materials and their performance on photocatalytic splitting of water, *J. Phys. Chem. C*, 2012, **116**, 1605–1613.

29 J. Wang, Y. Li, Z. Zhang and Z. Hao, Mesoporous KIT-6 silica-polydimethylsiloxane (PDMS) mixed matrix membranes for gas separation, *J. Mater. Chem. A*, 2015, **3**, 8650–8658.

30 K. De Sitter, P. Winberg, J. D'Haen, C. Dotremont, R. Leysen, J. A. Martens, S. Mullens, F. H. J. Maurer and I. F. J. Vankelecom, Silica filled poly(1-trimethylsilyl-1-propyne) nanocomposite membranes: relation between the transport of gases and structural characteristics, *J. Membr. Sci.*, 2006, **278**, 83–91.

31 S. Han, J. Xu, W. Hou, X. Yu and Y. Wang, Synthesis of high-quality MCM-48 mesoporous silica using gemini surfactant dimethylene-1,2-bis-(dodecyldimethylammonium bromide), *J. Phys. Chem. B*, 2004, **108**, 15043–15048.

32 R. Pierotti and J. Rouquerol, Reporting physisorption data for gas/solid systems with special reference to the determination of surface area and porosity, *Pure Appl. Chem.*, 1985, **57**, 603–619.

33 Y. P. Zhai, B. Tu and D. Y. Zhao, Organosilane-assisted synthesis of ordered mesoporous poly(furfuryl alcohol) composites, *J. Mater. Chem.*, 2009, **19**, 131–140.

34 B. Dou, Q. Hu, J. Li, S. Qiao and Z. Hao, Adsorption performance of VOCs in ordered mesoporous silicas with different pore structures and surface chemistry, *J. Hazard. Mater.*, 2011, **186**, 1615–1624.

35 A. L. Khan, C. Klaysom, A. Gahlaut, A. U. Khan and I. F. J. Vankelecom, Mixed matrix membranes comprising of Matrimid and -SO_3H functionalized mesoporous MCM-41 for gas separation, *J. Membr. Sci.*, 2013, **447**, 73–79.

36 T. S. Chung, L. Y. Jiang, Y. Li and S. Kulprathipanja, Mixed matrix membranes (MMMs) comprising organic polymers with dispersed inorganic fillers for gas separation, *Prog. Polym. Sci.*, 2007, **32**, 483–507.

37 H. Ren, J. Jin, J. Hu and H. Liu, Affinity between metal–organic frameworks and polyimides in asymmetric mixed matrix membranes for gas separations, *Ind. Eng. Chem. Res.*, 2012, **51**, 10156–10164.

38 D. Q. Vu, W. J. Koros and S. J. Miller, Mixed matrix membranes using carbon molecular sieves: II. Modeling permeation behavior, *J. Membr. Sci.*, 2003, **211**, 335–348.

39 Y. Li, T.-S. Chung, C. Cao and S. Kulprathipanja, The effects of polymer chain rigidification, zeolite pore size and pore blockage on polyethersulfone (PES)-zeolite A mixed matrix membranes, *J. Membr. Sci.*, 2005, **260**, 45–55.

40 B. D. Freeman, Basis of permeability/selectivity tradeoff relations in polymeric gas separation membranes, *Macromolecules*, 1999, **32**, 375–380.

41 S. Shahid and K. Nijmeijer, High pressure gas separation performance of mixed-matrix polymer membranes containing mesoporous Fe(BTC), *J. Membr. Sci.*, 2014, **459**, 33–44.

42 P. Duan, J. C. Moreton, S. R. Tavares, R. Semino, G. Maurin, S. M. Cohen and K. Schmidt-Rohr, Polymer infiltration into metal–organic frameworks in mixed-matrix membranes detected *in situ* by NMR, *J. Am. Chem. Soc.*, 2019, **141**, 7589–7595.

43 R. F. Boyer and R. L. Miller, Correlation of liquid-state compressibility and bulk mo1dulus with cross-sectional area per polymer-chain, *Macromolecules*, 1984, **17**, 365–369.